Nano Research

Open Access

Research Article

Tailored SnO_2 electron transport layer delivers over 27% external quantum efficiency in quantum dot light-emitting diodes compatible with multiple hole transport layers

Mengxin Liu[1], Chen lin[2], Heng Zhang[2], Xinan Shi[2] ✉, Ruosheng Zeng[2] ✉, and Daocheng Pan[1,2] ✉

[1] *School of Chemistry and Chemical Engineering, Guangxi University, Nanning 530004, China*
[2] *State Key Laboratory of Featured Metal Materials and Life-cycle Safety for Composite Structures; Guangxi Key Laboratory of Processing for Non-ferrous Metals and Featured Materials; Guangxi Key Laboratory of Advanced Rare Earth Materials; School of Resources, Environment and Materials, Guangxi University, Nanning 530004, China*

Cite this article: *Nano Research*, **2026**, *19*, 94908720. https://doi.org/10.26599/NR.2026.94908720

ABSTRACT: Achieving balanced charge transport is crucial for high-performance quantum-dot light-emitting diodes (QLEDs), yet it remains a significant challenge. This issue is notably evident when using high-mobility metal oxides, such as ZnO and SnO_2 nanoparticles, as electron transport layers (ETLs), due to their excessive electron mobility which leads to a severe mismatch with most organic hole transport layers (HTLs). Consequently, the balanced charge injection and high efficiency in conventional QLEDs have been largely confined to high-mobility HTLs like poly(9,9-dioctyl-fluorene-co-N-(4-butylphenyl) diphenylamine) (TFB). In this study, we present a universal strategy to precisely tune the electron mobility of SnO_2 nanocrystals through controlled Zn^{2+} doping concentration. This approach enables synergistic matching with a range of commonly used HTLs, achieving a near-ideal charge balance across all systems. As a result, we fabricated high-performance QLEDs with universal HTL compatibility, where all optimized devices exhibited a maximum external quantum efficiency (EQE) exceeding 27%. Importantly, the positive aging effect commonly observed in ZnMgO-based devices is completely eliminated in all our SnO_2-based QLEDs. This work provides a general and universal ETL materials for fabricating highly efficient and stable QLEDs compatible with diverse hole transport materials without the need to consider their hole mobility.

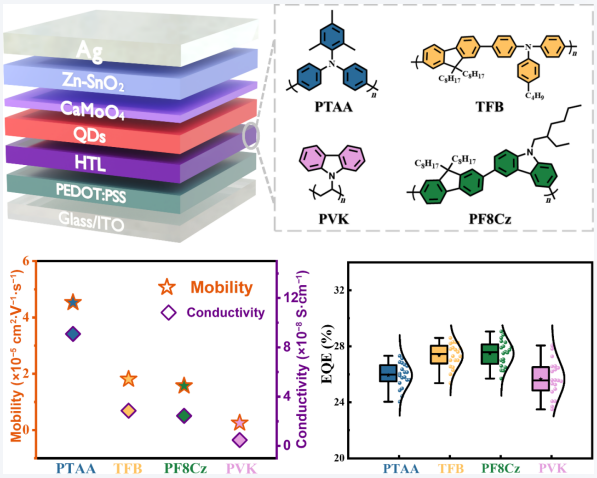

KEYWORDS: charge transport balance, quantum-dot light-emitting diode, tunable mobility, zinc doped tin dioxide, positive aging

1 Introduction

Quantum-dot light-emitting diodes (QLEDs) are considered a promising technology for next-generation high-definition displays and energy-efficient solid-state lighting, owing to their exceptional color purity, spectrally tunable emission, and potential for low-cost fabrication [1–9]. Over the past three decades, breakthroughs in quantum dot (QD) material synthesis and QLED device fabrication have pushed the external quantum efficiencies (EQEs) of red, green, and blue QLEDs beyond 20%, nearing their fundamental theoretical limits [10–15]. A typical high-performance QLED features a multilayer structure, including a transparent indium tin oxide (ITO) anode, a hole injection layer (HIL), a polymeric hole transport layer (HTL), a QD emitting layer (EML), a metal oxide electron transport layer (ETL), and a metal cathode [16–18]. The overall performance of QLEDs is critically dependent on the efficient injection and balanced transport of both holes and electrons into the QD EML. However, achieving this charge transport balance remains a formidable challenge, as it necessitates precise optimization of the energy level positions and charge

Received: January 23, 2026; **Revised:** April 2, 2026
Accepted: April 8, 2026

✉Address correspondence to Xinan Shi, xashi@gxu.edu.cn; Ruosheng Zeng, zengrsh@guet.edu.cn; Daocheng Pan, dcpan@gxu.edu.cn

transport properties of all functional layers. In this context, the ETL is particularly pivotal, as its characteristics are decisive in determining both the efficiency and operational stability of the QLEDs.

Currently, zinc oxide nanoparticles (ZnO NPs) have been widely used as the ETL in high-performance QLEDs [10–27], but their inherent chemical instability, abundant surface defects, and unfavorable positive aging effects pose significant challenges to the long-term operational stability and commercial viability [19–27]. Consequently, alternative metal oxide ETLs such as tin dioxide (SnO_2) NPs have attracted considerable attention due to their superior chemical stability, high electron mobility, and excellent optical transparency [28–43]. Nonetheless, the relatively high electron mobility of SnO_2 NPs which far surpasses the hole mobility of common organic HTLs will induce severe charge imbalance in QLEDs. This imbalance promotes excessive electron accumulation in the QD EML and exacerbates non-radiative Auger recombination, ultimately constraining device efficiency and operational lifetime [41–43]. Meanwhile, the electron mobility of ZnO NP is difficult to precisely regulate over a wide range. As a result, high-efficiency ZnO-based QLEDs can only be fabricated using high-hole-mobility poly(9,9-dioctyl-fluorene-co-N-(4-butylphenyl) diphenylamine) (TFB) as the HTL. Therefore, it is highly desirable to achieve wide-range and precise regulation of the electron mobility in SnO_2 NPs to match diverse organic HTL materials with different hole mobilities.

To address this challenge, our previous work demonstrated that substituting Sn^{4+} ions with Zn^{2+} ions can effectively reduce the electron mobility and conductivity of SnO_2 NPs, thereby improving charge transport balance [42]. Building on this finding, we herein propose a systematic strategy to modulate the electron transport properties of SnO_2 NPs through controlled Zn doping concentrations (5%–10%), aiming to achieve compatibility with four distinct HTLs, including TFB, (poly[bis(4-phenyl) (2,4,6-trimethylphenyl) amine) (PTAA), poly((9,9-dioctylfluorenyl-2,7-diyl)-alt-(9-(2-ethylhexyl)-carbazole-3,6-diyl)) (PF8Cz), and poly(9-vinylcarbazole) (PVK). Note that these HTLs were selected for their varied hole mobilities, conductivities, and energy level alignments. By fine-tuning the electron mobility of Zn-doped SnO_2 NPs, we can effectively match four types of HTLs with tailored Zn-doped SnO_2 NP ETLs, realizing a charge transport balance in all HTL systems and thereby minimizing carrier accumulation and enhancing radiative recombination. Although the hole injection mechanism in QLEDs has recently been reexamined [44], the intentional modulation of ETL properties to match specific HTL remains underexplored. In this work, we demonstrate that precisely controlling the electron mobility and conductivity of Zn-SnO_2 NPs enables near-ideal charge transport balance across all four HTL systems, leading to consistently high device performance. All corresponding QLEDs exhibited maximum EQE exceeding 27%, with the highest reaching 29.1%, which is the highest value reported to date for SnO_2-based QLEDs. This work not only provides a versatile ETL material for fabricating high-efficiency and positive aging-free QLEDs but also offers valuable insights into the design principles of charge transport-balanced optoelectronic devices.

2 Experimental section

2.1 Materials

Anhydrous zinc acetate ($Zn(OAc)_2$, 99%), anhydrous tin tetrachloride ($SnCl_4$, 99.9%), ethanolamine (99%), diethanolamine (99%), propionic acid (99%), propylamine (99%), n-butyric acid (99%), and n-butylamine (99%) were bought by MACKLIN Inc. Methanol (A.R.), ethanol (A.R.), ethyl acetate (99.5%), and acetonitrile (A.R.) were purchased from Chengdu Kelong Chemicals Inc. Calcium nitrate ($Ca(NO_3)_2{\cdot}4H_2O$, 99%) and ammonium molybdate ($(NH_4)_6Mo_7O_{24}{\cdot}4H_2O$, 99.5%) were supplied by Beijing Chemical Factory. Red-emitting CdSe/ZnSe/ZnS core/shell/shell quantum dots (10 mg·mL^{-1} in hexane) and ZnMgO NPs (50 mg·mL^{-1} in ethanol) were purchased from Poly Optoelectronics Inc. Poly-(ethylenedioxythiophene):polystyrene-sulfonate (PEDOT:PSS, Al 4083), PTAA, ($M_W \approx 15$–25 k), poly(9,9-dioctyl-fluorene-co-N-(4-butylphenyl)diphenylamine) ($M_W \approx 20$–40 k), poly((9,9-dioctylfluorenyl-2,7-diyl)-alt-(9-(2-ethylhexyl)-carbazole-3,6-diyl)), poly(N,N'-bis(4-butylphenyl)-N,N'-bis(phenyl)benzidine] (poly-TPD, $M_W \approx 25$–35 k), and poly(9-vinylcarbazole) ($M_W \approx 20$ k) were purchased from Xi'an Polymer Light Technology Co. Ltd. All chemicals were used directly without any further purification.

2.2 Synthesis of Zn-SnO_2 nanoparticles

Zn-SnO_2 NPs were synthesized by a solvothermal method [42]. In a typical synthesis, 2.5 mL of butyric acid, 2.5 mL of butylamine, and 25 mL of ethanol were mixed in a beaker and stirred for 5 min to form a clear solution. Subsequently, appropriate amounts of $SnCl_4$ and $Zn(OAc)_2$ were added to the above solution. The doping ratios of Zn^{2+} were 5%, 7.5%, and 10%, respectively, while the total molar amount of metal precursors (Sn^{4+}+Zn^{2+}) was maintained at 5.0 mmol. Under magnetic stirring, the mixture was transferred into a 50 mL of Teflon-lined stainless-steel autoclave, which was then sealed and heated in an oven at 120 °C for 12 h. After the reaction, the autoclave was allowed to cool naturally to room temperature. The white precipitate was collected by centrifugation and washed twice with ethanol. Subsequently, the obtained white precipitate was mixed with 10 mL of ethanol and 1.0 mL of ethanolamine and then was treated in an ultrasonic bath until the formation of a clear and transparent colloidal solution. After further purification with ethyl acetate and ethanol, the final ethanolamine-capped Zn-SnO_2 nanoparticles were dispersed in 20.0 mL of ethanol.

2.3 Synthesis of $CaMoO_4$ nanoparticles

$CaMoO_4$ NPs were synthesized according to our recently reported method with some modifications [42]. Under magnetic stirring, 5.0 mmol of $Ca(NO_3)_2$ was dissolved in a solution of 5.0 mL of propionic acid and 5.0 mL of propylamine in ethanol until the solution became clear and transparent. $(NH_4)_6Mo_7O_{24}$ (5.0 mmol of MoO_4^{2-}) was dissolved in a mixed solvent containing 20 mL of methanol and 5.0 mL of propylamine using an ultrasonic bath. Subsequently, the two clear solutions were mixed and allowed to react for 1 min at room temperature with magnetic stirring. Appropriate amount of acetonitrile was added as an anti-solvent to induce precipitation, and the white solid was collected by centrifugation. Then, 20 mL of ethanol and 2.0 mL of diethanolamine were added, and ligand exchange was carried out in an ultrasonic bath until a clear and transparent solution was formed. Finally, the $CaMoO_4$ NPs were washed with ethyl acetate and then were redispersed in ethanol.

2.4 Device fabrication

Pre-cleaned ITO glass substrates were treated with oxygen plasma

for 10 min to improve surface wettability and remove organic contaminants. A PEDOT:PSS solution was spin-coated onto the ITO glass at 3000 rpm for 40 s, followed by heating process at 130 °C for 30 min in air. Subsequently, the HTL material (8 mg·mL^{-1} in chlorobenzene) was spin-coated at 3000 rpm and baked inside a nitrogen-filled glovebox. The QD solution was then deposited by spin-coating at 1200 rpm for 30 s. Afterwards, the $CaMoO_4$ NP solution (1.6 mg·mL^{-1} in ethanol) was spin-coated at 3000 rpm for 40 s and baked at 100 °C for 8 min. Subsequently, the Zn-SnO_2 NP solution (30 mg·mL^{-1}) was spin-coated at 3000 rpm for 30 s and baked at 100 °C for 10 min. Next, a 100 nm Ag cathode was thermally evaporated under high vacuum (5×10^{-4} Pa). Finally, QLED devices were encapsulated using an ultraviolet (UV)-curable epoxy resin and a cover glass.

2.5 Characterizations

The ultraviolet photoelectron spectroscopy (UPS) measurements were obtained on Thermo Fisher Escalab 250Xi equipped with a monochromatic Al Kα radiation. The MFP-3D-SA system (Asylum Research) was used to obtain the tapping-mode atomic force microscopy (AFM) images. The thickness of the thin film was measured by a step profiler (KLA Tencor, D-100). The PL spectra were characterized by an Edinburgh FS5 spectrofluorometer. Ultraviolet–visible (UV–vis) absorption spectra were measured using a UV-5200PC spectrometer. The conductivity of the thin film was acquired using an Agilent B1500A semiconductor parameter analyzer by using a two-electrode method [43]. The work function was measured by a Kelvin Probe system (KP Technology, APS04-N2-RH). QLED performance (*J*–*V*–*L* and EQE–*L* curves) was measured by a commercialized QLED measurement system (XPQY-EQE-Adv, Guangzhou Xi Pu Optoelectronics Technology Co., Ltd.), which was equipped with an integrated sphere and an Ocean Optics QE Pro spectrometer. QLED lifetime was recorded by a QLED life measurement system (XP-LTS-8, Guangzhou Xi Pu Optoelectronics Technology Co., Ltd.).

3 Results and discussion

As shown in Fig. 1(a), the fabricated QLED adopts a multilayer structure of glass/ITO/PEDOT:PSS (20 nm)/organic HTLs (30 nm)/QDs (13 nm)/$CaMoO_4$ (6 nm)/Zn-SnO_2 (45 nm)/Ag. In this configuration, Zn-SnO_2 NPs serve as ETL, while $CaMoO_4$ NPs are introduced as an interfacial modification layer (IML) between the ETL and the QD emissive layer, with the primary purpose of suppressing interfacial exciton quenching and non-radiative recombination rather than regulating bulk charge transport [42]. Four polymeric HTL materials, including PTAA, TFB, PF8Cz, and PVK, were employed, with their chemical structures shown in Fig. 1(b). The Zn-SnO_2 NPs were synthesized via a solvothermal method assisted by butyric acid and butylamine (see Experimental section for details). The substitution of Sn^{4+} ions by Zn^{2+} ions can effectively decrease the electrical conductivity and electron mobility of the SnO_2 NPs. By precisely tuning the Zn^{2+} doping concentration (5%, 7.5%, 10%), we modulated the electronic properties of the SnO_2 NPs to achieve compatibility with the four organic HTLs, thereby promoting favorable energy-level alignment and charge transport balance, which is essential for high-performance QLEDs. With increasing Zn^{2+} doping concentrations, both the electron mobility and conductivity of SnO_2 NPs decreased significantly due to the reduced free electron concentration induced by Zn^{2+} substitution. The electron mobility dropped from 2.7×10^{-4} to 8.4×10^{-5} cm^2·V^{-1}·s^{-1}, while the conductivity decreased from 1.8×10^{-5} to 2.9×10^{-6} S·cm^{-1} [42]. This downward trend is further corroborated by electron-only devices (EODs, structure illustrated in Fig. S1 in the Electronic Supplementary Material (ESM)), which exhibited a corresponding decrease in current density at higher Zn^{2+} doping concentration. AFM characterizations confirmed that all Zn-SnO_2 NP thin films were dense and smooth, with a surface roughness of approximately 1.0 nm (Fig. S2 in the ESM). The energy level diagram for each functional layer of the QLED device is presented in Fig. 1(c). Notably, the doping of Zn^{2+} ions can effectively widen the bandgap and elevate the conduction band minimum (CBM) position of SnO_2 NPs, as evidenced by optical bandgap and UPS measurements (Figs. S3 and S4 in the ESM). This upward shift in CBM increases the electron injection barrier at the Ag cathode, thus effectively suppressing electron injection into the QD EML (Fig. S5 in the ESM).

The conductivity and hole mobility of the four HTL materials (PTAA, TFB, PF8Cz, and PVK) were systematically characterized, as summarized in Figs. 1(d) and 1(e). PTAA exhibits the highest conductivity (9.09×10^{-8} S·cm^{-1}) and hole mobility (4.53×10^{-5} cm^2·V^{-1}·s^{-1}), followed by TFB and PF8Cz, as shown in Fig. 1(e) and Fig. S6 in the ESM. In contrast, PVK shows markedly inferior hole transport properties, with a conductivity of only 4.76×10^{-9} S·cm^{-1} and a hole mobility of 2.52×10^{-6} cm^2·V^{-1}·s^{-1} (see Fig. 1(e) and Fig. S6 in the ESM). These substantial differences in electrical properties critically influence the hole injection efficiency and overall charge balance within the QLEDs. Therefore, the charge transport balance can be achieved by tailoring the electron mobility and conductivity of Zn-SnO_2 NPs to match the specific hole transport characteristics of each HTL material.

Photoluminescence (PL) spectroscopy was employed to further evaluate the hole injection efficiency from the various HTLs into the QD layer. The optimal excitation wavelength for each HTL was determined from UV–vis absorption spectra (Fig. S7 in the ESM). As shown in Fig. S8 in the ESM, the intrinsic fluorescence emission bands of the four HTL films (PTAA, TFB, PF8Cz, and PVK) are concentrated in the range of 380–550 nm. This region is well-separated spectrally from the emission of the QDs (627 nm), thereby minimizing spectral overlap and enabling a clear analysis of the interfacial hole injection process. After depositing the QD layer onto each HTL, a pronounced quenching of the HTL photoluminescence was observed. This PL quenching phenomenon is typically attributed to efficient charge transfer at the HTL/QD interface, which leads to the effective quenching of excitons generated in the HTL. Therefore, the hole injection capability can be quantitatively evaluated by calculating the photoluminescence quenching efficiency (PLQE) of the HTL, where a higher PLQE value corresponds to a greater hole injection efficiency. The PLQE is defined by the following formula [45]

$$\mathrm{PLQE} = 1 - \frac{\eta_{\mathrm{HTL/QDs}}}{\eta_{\mathrm{HTL}}} \quad (1)$$

where η_{HTL} and $\eta_{\mathrm{HTL/QDs}}$ represent the integrated PL intensities of the pristine HTL film and the HTL/QD bilayer, respectively. The calculated PLQE values of the HTL/QD bilayers containing PTAA, TFB, PF8Cz, and PVK are 0.563, 0.538, 0.519, and 0.230, respectively. These results confirm that the hole injection efficiency follows the order of PTAA > TFB > PF8Cz > PVK, which is fully consistent with the trend previously observed in Fig. 1(e).

The superior electrical performance of PTAA originates from its

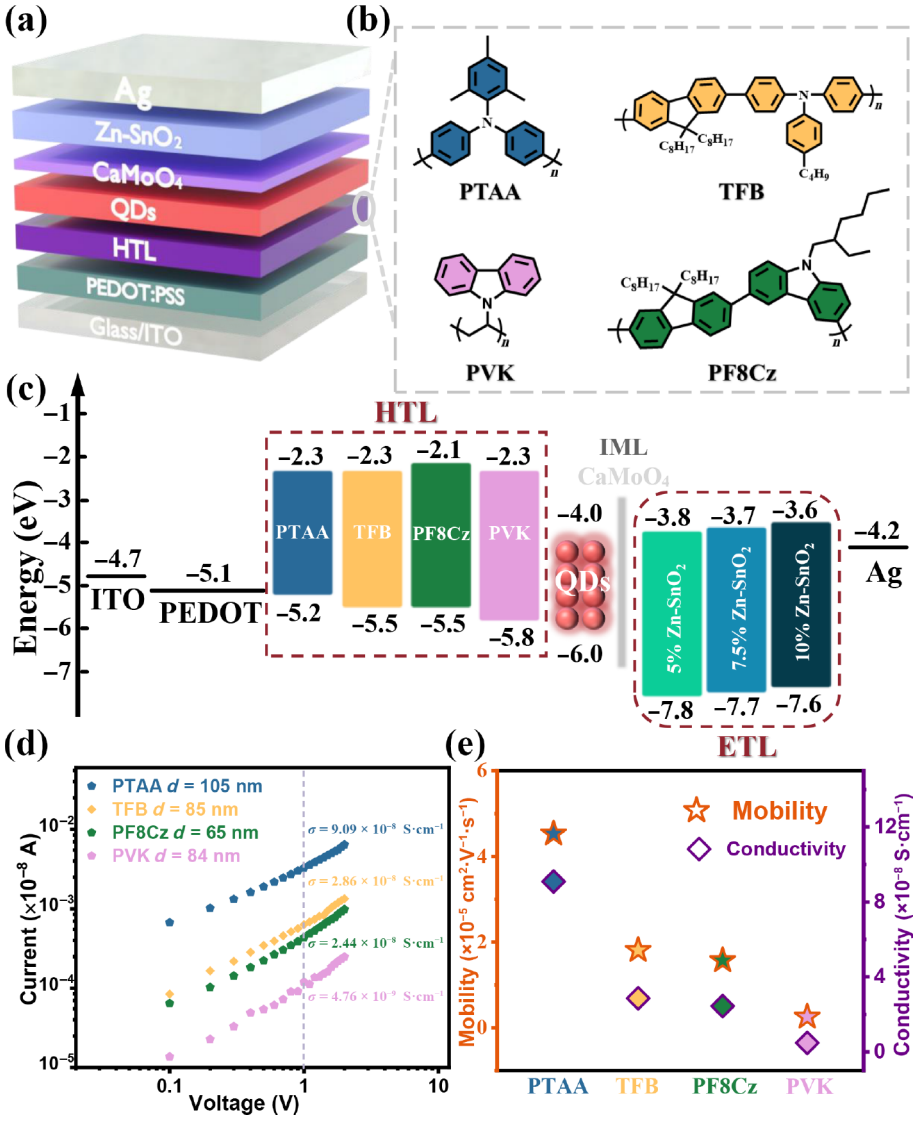

Figure 1 (a) Schematic device structure. (b) Chemical structures of PTAA, TFB, PF8Cz, and PVK. (c) The energy level diagram for each functional layer of the QLED device. (d) *I*–*V* curves of ITO/HTLs (PTAA, TFB, PF8Cz, PVK)/MoO_3/Al devices. (e) The hole mobility and conductivity of different HTL (PTAA, TFB, PF8Cz, PVK) thin films.

favorable molecular packing and extended conjugation, which promote highly efficient intrachain charge transport [46]. However, its relatively shallow highest occupied molecular orbital (HOMO) level introduces a substantial hole-injection barrier at the interface, limiting hole transfer to the QDs and potentially compromising device performance and operational stability [47]. In contrast, TFB and PF8Cz exhibit balanced electrical properties, combining good conductivity and hole mobility with well-aligned HOMO levels. These characteristics significantly enhance hole injection efficiency, reduce non-radiative recombination losses, and promote improved charge transport balance with electrons injected from the tailored Zn-SnO_2 ETL. Conversely, the low-mobility and high-resistivity PVK leads to insufficient hole transport and imbalanced charge injection, which adversely affects device efficiency and stability. To overcome these challenges of energy-level mismatch and charge transport imbalance, we propose a systematic approach that involves precise modulation of the electron transport properties of Zn-SnO_2 ETL, coupled with the selection of an appropriate HTL possessing matched mobility and conductivity. Finally, the charge transport balance can be realized in four HTL systems. This synergistic engineering strategy can effectively suppress Auger recombination and enhance radiative recombination, providing a reliable route to high-performance QLEDs.

To validate the proposed strategy, we fabricated a series of QLEDs by systematically pairing four types of HTLs with tailored SnO_2 ETLs doped with different concentrations of Zn^{2+} ions. Figure S9 in the ESM displays the electroluminescence (EL) spectra of QLEDs utilizing four different HTL materials under a driving voltage of 5.0 V. All EL spectra exhibit a characteristic emission peak at 627 nm with a full width at half maximum (FWHM) of 24 nm. As illustrated in the current density–voltage–luminance (*J*–*V*–*L*) characteristics (Figs. 2(a)–2(d) and Fig. S10 in the ESM), the current density at a fixed voltage decreases consistently with increasing Zn^{2+} doping concentration for each HTL system. Among the optimized devices, the PTAA-based QLED exhibited the lowest turn-on voltage (V_{on}) of 1.7 V, attributable to its outstanding conductivity and hole mobility. The V_{on} values for TFB-, PF8Cz-, and PVK-based QLED devices were 1.8, 2.1, and 2.7 V, respectively.

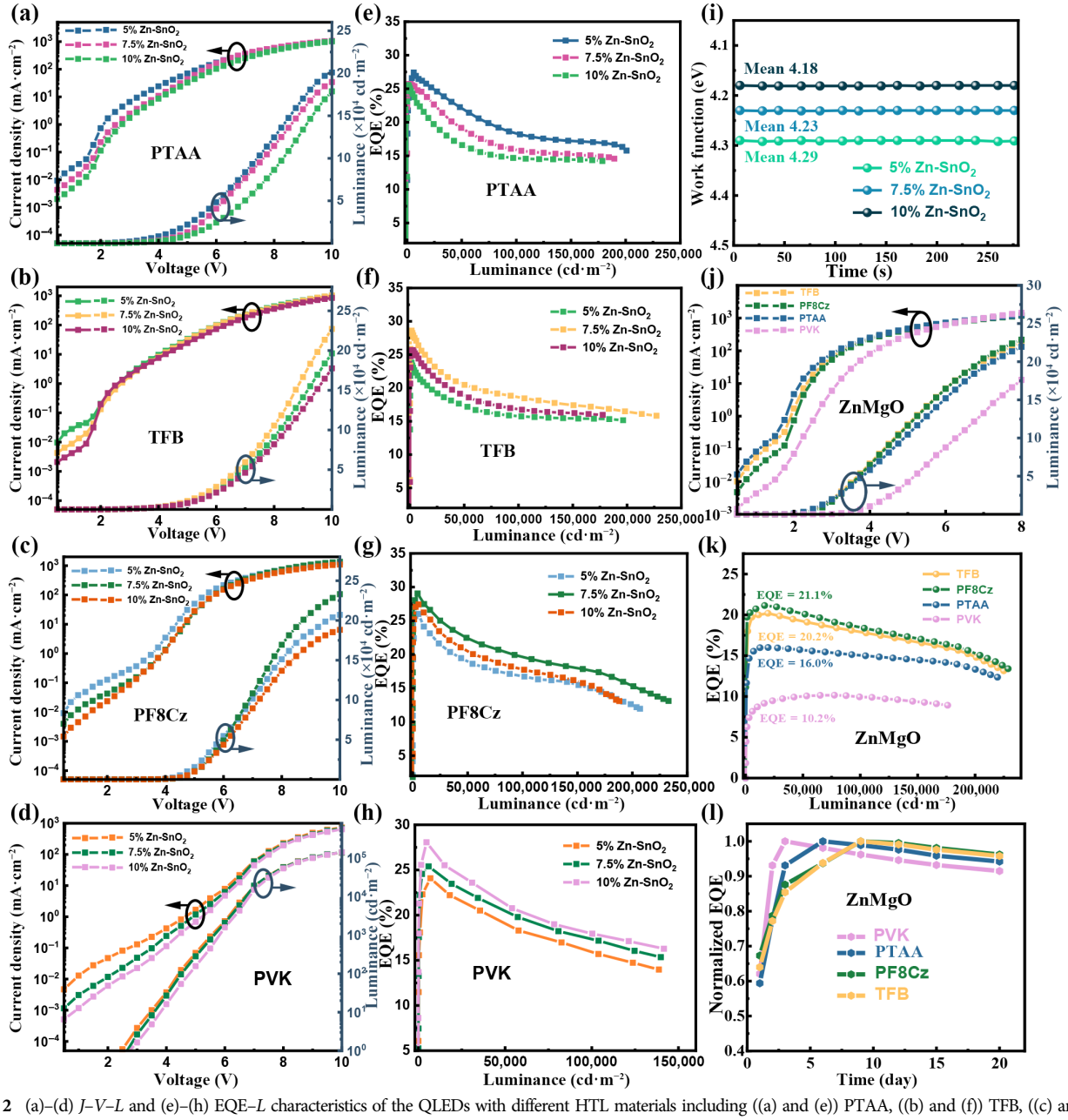

Figure 2 (a)–(d) *J*–*V*–*L* and (e)–(h) EQE–*L* characteristics of the QLEDs with different HTL materials including ((a) and (e)) PTAA, ((b) and (f)) TFB, ((c) and (g)) PF8Cz, and ((d) and (h)) PVK with different Zn doping concentrations. (i) Work functions of Zn-doped SnO_2 NPs calculated by using the contact potential difference (CPD) results detected by Kelvin probe (ITO with a work function of 4.7 eV is used as the reference specimen). (j) *J*–*V*–*L* and (k) EQE–*L* characteristics as well as (l) the positive aging effect tests of ZnMgO-based QLED devices with PTAA, TFB, PF8Cz, and PVK as the HTLs.

All fabricated devices exhibited exceptionally high luminance. Specifically, the PTAA-based QLED with a 5% Zn-doped SnO_2 NP ETL achieved a maximum luminance of 200,901 cd·m^{-2} and a peak EQE of 27.4%, as shown in Figs. 2(a) and 2(e) and Table S1 in the ESM. Devices incorporating TFB and PF8Cz as HTLs and 7.5% Zn-doped SnO_2 NPs as ETL attained even higher maximum luminance values of 227,118 and 232,989 cd·m^{-2}, respectively (Figs. 2(b) and 2(c) and Table S1 in the ESM), benefiting from their suitable energy levels and good hole mobility. The PF8Cz-based QLED device obtained a superior EQE of 29.1% compared to the TFB-based device with an EQE of 28.6% (Figs. 2(f) and 2(g) and Table S1 in the ESM). This performance advantage is attributed to the shallower lowest unoccupied molecular orbital (LUMO) level of PF8Cz, which effectively suppresses electron leakage from the quantum dot layer into the HTL, thereby reducing non-radiative recombination [2]. In previous reports [48–50], PVK-based QLEDs usually suffered from severe charge transport imbalance due to the low conductivity and poor hole mobility of PVK, which induces severe non-radiative Auger recombination and leads to very poor device performance. By increasing the Zn^{2+} doping ratio in the SnO_2 ETL from 5% to 10%, we effectively reduced its conductivity and electron mobility while lowering its work function from 4.29 to 4.18 eV, as shown in Fig. 2(i). This modulation raised the electron injection barrier and alleviated electron accumulation in QD layer, thereby restoring charge transport balance. As a result, the optimized PVK-based QLED achieved a maximum luminance of 140,595 cd·m^{-2} and a peak EQE of 28.1% (Figs. 2(d) and 2(h) and Table S1 in the ESM). Furthermore, we extended this approach to

poly-TPD as an additional HTL with the optimized 7.5% Zn-doped SnO_2 NPs, achieving a maximum EQE of 25.5% (see Fig. S11 in the ESM). These collective results demonstrate that our mobility-tunable Zn-SnO_2 nanocrystals exhibit broad compatibility and can be effectively matched with various organic HTLs to produce high-efficiency QLEDs.

For comparison, we also fabricated QLEDs using ZnMgO NPs as ETL in combination with fivefour organic HTL materials with different hole mobilities. Their *J*–*V*–*L* and EQE–*L* curves are shown in Figs. 2(j) and 2(k), respectively. Since the electron mobility of ZnMgO NPs cannot be precisely regulated over a wide range and is significantly higher than the hole mobilities of most organic hole transport materials, highly efficient ZnMgO-based QLEDs could only be achieved using high-hole-mobility materials such as TFB and PF8Cz. As shown in Fig. 2(k), the maximum EQEs of PF8Cz- and TFB-based QLEDs were 21.1% and 20.2%, respectively, while the PTAA-based device reached 16.0%. In contrast, the low-hole-mobility PVK exhibited maximum EQEs of only 10.2%. These results indicate that the ZnMgO ETL lacks broad compatibility with diverse organic HTL materials. Additionally, we investigated the positive aging behavior of these four types of devices. After encapsulation with an acidic UV-curable resin, the devices were stored in ambient air, and their EQE was monitored over time. As shown in Fig. 2(l), all ZnMgO-based devices exhibited a significant positive aging effect. Their EQE values increased with storage time, peaking within several days, with enhancement factors ranging from 1.48 to 1.97. In contrast, no such positive aging effect was observed in our SnO_2-based QLEDs.

To assess device reproducibility, we fabricated and characterized 20 individual SnO_2-based devices from different batches for each of the four HTL materials, all employing their respective optimized Zn-doped SnO_2 ETLs. As summarized in Fig. 3(a), the QLEDs based on TFB and PF8Cz HTLs consistently delivered superior performance, yielding average maximum external quantum efficiencies of 27.3% and 27.5%, respectively. In comparison, QLED devices with PVK and PTAA as the HTL showed slightly lower average maximum EQEs of 25.7% and 26.0%. These results confirm the excellent reproducibility of our QLEDs across all four HTL systems. Remarkably, we achieved a champion EQE of 29.1% (Fig. 3(b)), to the best of our knowledge, which represents the highest value reported to date for SnO_2-based QLEDs. Moreover, we systematically compared the device performance using undoped SnO_2 and Zn-doped SnO_2 as the ETLs (see Fig. S12 in the ESM). The results indicate that Zn^{2+} doping plays a crucial role in regulating internal charge transport balance and enhancing the overall device performance.

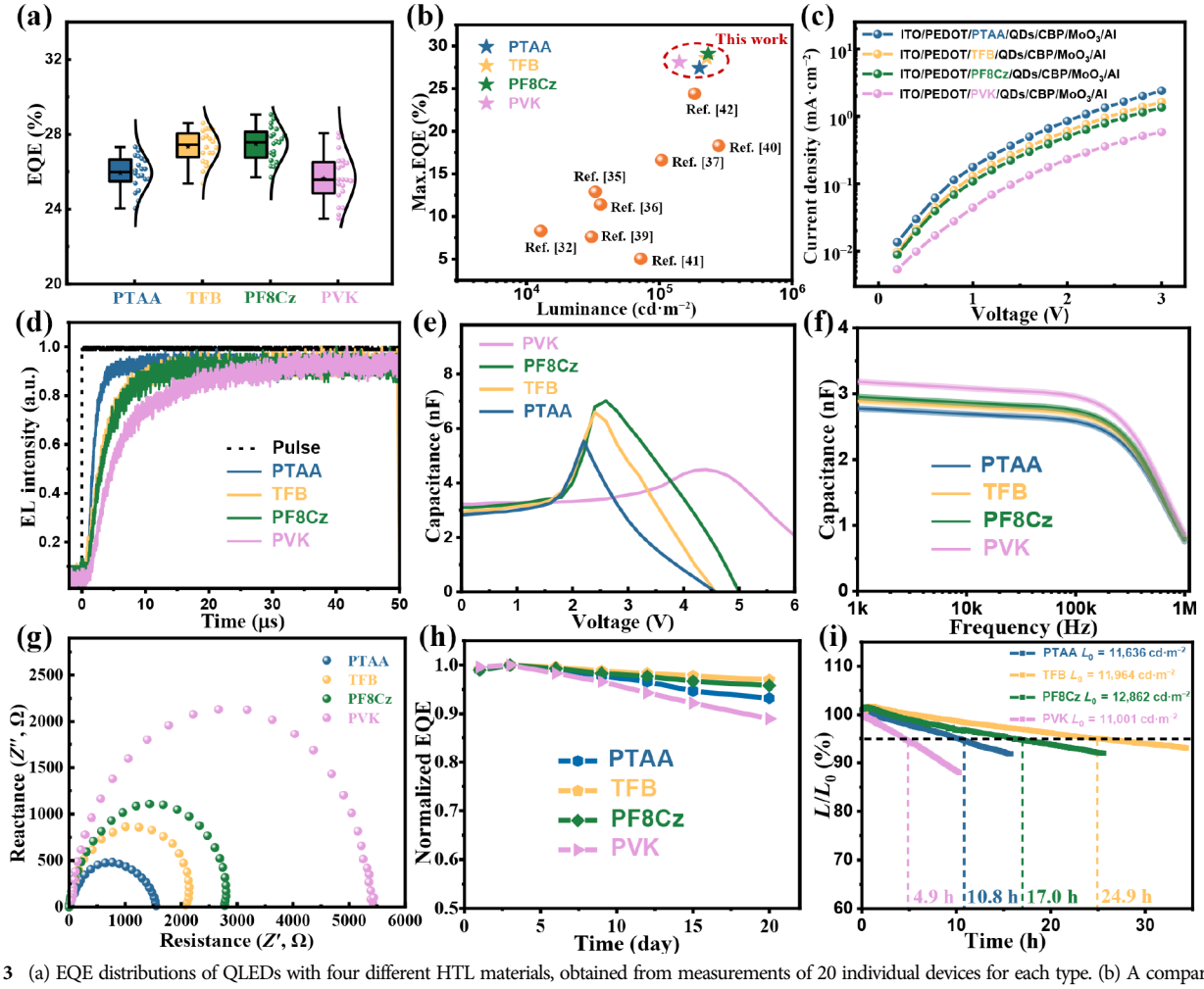

Figure 3 (a) EQE distributions of QLEDs with four different HTL materials, obtained from measurements of 20 individual devices for each type. (b) A comparison of the maximum EQEs achieved in this work with previously reported values in the literature. (c) *J*–*V* curves of the HODs with structure of ITO/HIL/HTLs/QDs/CBP/MoO_3/Al. (d) TREL spectra, (e) *C*–*V*, (f) *C*–*f*, (g) Nyquist curves, (h) the shelf stability measurements, and (i) the device operational lifetimes of the QLEDs with different HTL materials, all of which use 7.5% Zn-doped SnO_2 NPs as the ETL.

To further investigate the hole transport properties of the four HTLs, we constructed corresponding hole-only devices (HODs, structure illustrated in Fig. 3(c)). Current density measurements revealed that the PTAA-based HOD achieved the highest current density, attributable to its superior conductivity and hole mobility. In contrast, the PVK-based device exhibited the lowest current density, reflecting its limited hole injection capability. Transient electroluminescence (TREL) measurements were subsequently performed on the complete QLEDs to probe carrier dynamics (Fig. 3(d)). By employing an identical Zn-doped SnO_2 NPs as the ETL across all devices, the observed differences can be uniquely attributed to the various HTLs. The rise time of the TREL signal, which reflects the combined timescale of carrier injection, transport, and exciton formation, was markedly shorter in the devices with PTAA (13.1 μs), TFB (16.7 μs), and PF8Cz (18.1 μs) HTLs compared to the PVK-based device (34.3 μs). The faster electro-optical response of the first three HTLs-based QLEDs aligns well with their higher current densities observed in HODs (Fig. 3(d)), collectively confirming their efficient hole injection and rapid transport characteristics. Conversely, the slow TREL response of the PVK-based device further highlights its inadequate hole injection and transport capability.

To probe charge carrier accumulation and recombination in the QLEDs, we characterized the capacitance–voltage (*C*–*V*) characteristics of the devices with the four different HTLs (Fig. 3(e)). The *C*–*V* curves exhibit distinct peak shapes that strongly depend on the HTL material. Devices with PTAA, TFB, and PF8Cz HTLs show relatively high and sharp capacitance peaks, indicating efficient charge transport and consequently more effective charge accumulation and recombination. Among them, PTAA, which possesses the highest hole mobility, enables the most efficient hole injection and transport. This leads to a more balanced electron-hole carrier flux within the device, thereby effectively reducing hole accumulation at the HTL/QD interface and resulting in the lowest capacitance peak. In contrast, the PVK-based device exhibits an anomalously low and broad capacitance peak. This can be attributed to the extremely low hole mobility of PVK, which severely limits the number of holes reaching the QD interface, thereby suppressing large-scale charge accumulation and resulting in a low capacitance peak. The broadened peak profile is likely caused by the abundance of trap states in the PVK film, which captures charge carriers across a wide voltage range and thus leads to a dispersed charge accumulation process [51]. To further resolve the spatial capacitance behavior, we measured the capacitance–frequency (*C*–*f*) characteristics of four types of QLEDs under zero bias (Fig. 3(f)). In the low-frequency region (< 100 kHz), the device capacitance remains stable at the geometric capacitance due to the absence of carrier injection, and decays rapidly near 1 MHz. Notably, the PVK-based device displayed the highest capacitance of 3.19 nF at 1 kHz among all devices. This elevated capacitance suggests that PVK as the HTL introduces a higher series resistance, which more strongly suppresses carrier injection and modulates the dielectric response [52–54]. To exclude the potential influence of capacitive effects on the device performance evaluation, we performed ten consecutive *J*–*V*–*L* scans and an EQE stability test on the PVK-based QLED (see Fig. S13 in the ESM). The results confirm that the high efficiency of the PVK-based device is intrinsic and not attributable to its higher capacitance. Furthermore, impedance analysis (Fig. 3(g)) reveals that the recombination resistance and reactance of the devices correlate directly with the conductivity and mobility of their functional layers. A reduction in internal resistance can effectively decrease the time constant of the device, which is crucial for enhancing the electron-hole recombination efficiency.

Although the positive aging effect in SnO_2-based QLEDs has been effectively mitigated, the intrinsic chemical instability of the organic HTL remains a critical factor limiting device shelf stability. To systematically evaluate this issue, we encapsulated the QLED devices with an acidic UV-curable adhesive and monitored their performance after 20 days of storage in ambient air. As shown in Fig. 3(h), no positive aging effects were observed in all of the SnO_2-based QLED devices, regardless of the hole transport material used, as their EQEs exhibited a monotonic decrease, which are totally different from those of ZnMgO-based QLEDs (see Fig. 2(l)). The devices employing TFB and PF8Cz as the HTL exhibited exceptional stability, retaining 97% and 96% of their initial efficiency, respectively. This outstanding performance is critically important for the commercial prospects of QLED displays. We attribute this robustness to the polyfluorene units within the TFB and PF8Cz copolymers, which not only forms a rigid backbone that improves solubility and film formation but also provides strong inherent hydrophobicity, effectively blocking the penetration of ambient moisture and oxygen. In contrast, PVK-based QLED showed the poorest stability, with only 89% efficiency retention. This poor stability is likely attributed to PVK's structure as a side-chain homopolymer, which facilitates the exposure of active sites and offers insufficient steric hindrance, thereby increasing its susceptibility to water and oxygen.

The operational stability of the four HTLs-based QLEDs was evaluated by measuring the luminance decay lifetime under constant current driving (Fig. 3(i)). To exclude the influence of the ETL, all comparison devices used an identical 7.5% Zn-doped SnO_2 NPs as the ETL, thereby enabling a systematic investigation of the effect of different HTLs on device lifetime. As anticipated, the TFB-based device demonstrated the best stability, with a T_{95} lifetime (time for luminance to decay to 95% of the initial value) of 24.9 h from an initial luminance of 11,964 cd·m^{-2}. When standardized to 1000 cd·m^{-2} using an acceleration factor of 1.72, the TFB-based device achieved a longest T_{95} lifetime of 1778.9 h, significantly surpassing those of PF8Cz- (1375.5 h) and PTAA-based (735.5 h) devices. In contrast, the PVK-based device showed the poorest operational stability, with a T_{95} lifetime of only 303.0 h. To explore the underlying reasons for these pronounced stability differences, we hypothesized that, in addition to the intrinsic chemical stability of the HTL materials, the internal resistance of the QLED device should play a critical role. We therefore monitored the surface temperature evolution of the devices during operation using an infrared thermal camera (Fig. 4). After one hour of continuous operation at 1000 cd·m^{-2}, the temperatures of TFB-, PTAA-, and PF8Cz-based devices remained nearly unchanged. However, the PVK-based device exhibited a temperature increase of 1.2 °C due to its higher internal resistance. At a higher luminance of 5000 cd·m^{-2}, the temperature difference became more pronounced, and the PVK-based device reached 34.5 °C, whereas the TFB-based device remained at only 26.8 °C. These results clearly indicate that a lower internal resistance can effectively suppress Joule heat accumulation during device operation, which is essential for improving the operational stability of QLEDs. Moreover, Zn doping effectively promotes overall charge transport balance and significantly suppresses non-radiative recombination, which positively contributes to the overall thermal stability of the device, as shown in

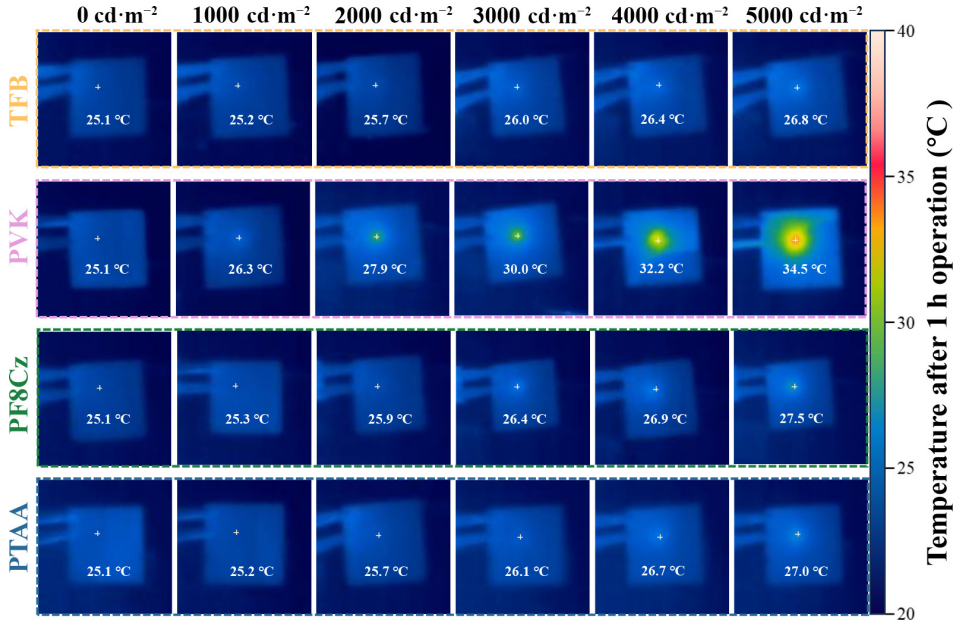

Figure 4 Surface temperature profiles of QLEDs employing different HTL materials, measured by infrared thermography after 1.0 h of continuous operation at an ambient temperature of 25.1 °C.

Fig. S14 in the ESM. Therefore, future research should aim to develop high-conductivity ETLs and HTLs with closely matched electron and hole mobilities to achieve balanced charge transport and suppress Joule heat.

4 Conclusions

In summary, we have developed a highly effective and universal strategy to achieve near-ideal charge transport balance in QLEDs through the synergistic engineering of the electron transport layer and the rational selection of a compatible hole transport layer. By modulating the Zn^{2+} doping concentration, the electron mobility and conductivity of Zn-doped SnO_2 nanoparticles can be tailored over a wide range. This enables the electron supply rate to be precisely matched to the hole injection capabilities of four distinct HTL materials (PTAA, TFB, PF8Cz, and PVK). Such matching effectively alleviates electron accumulation, suppresses non-radiative losses, and enhances radiative recombination across all HTL systems. Consequently, we fabricated a series of high-performance QLEDs, all of which achieved maximum EQEs exceeding 27%. Notably, a champion device employing a PF8Cz HTL reached a record EQE of 29.1%. Our results demonstrate that the external quantum efficiency of QLEDs is governed by the charge transport balance, while the operational stability is dictated by the resistivity of the hole and electron transport layers. These insights provide a foundational guideline for designing and synthesizing next-generation charge transport materials.

Electronic Supplementary Material: Supplementary material (*J*–*V* curves of EODs, AFM surface morphologies, UV–vis, UPS, PL, and EL spectra, illustration of the electron injection and recombination processes, conductivity and electrical characteristics of HTLs, detailed device parameters, QLED performance tests including *J*–*V*–*L* and EQE–*L* curves, stability tests, as well as surface temperature profiles measured by infrared thermography) is available in the online version of this article at https://doi.org/10.26599/NR.2026.94908720.

Data availability

All data needed to support the conclusions in the paper are presented in the manuscript and the Electronic Supplementary Material. Additional data related to this paper may be requested from the corresponding author upon request.

Acknowledgements

This work was supported by grants from the Natural Science Foundation of Guangxi (No. 2026GXNSFAA00641054) and Guangxi Science and Technology Major Project (Nos. ZY24212006 and AA23073018).

Declaration of competing interest

All the contributing authors report no conflict of interests in this work. Author Ruosheng Zeng is the editorial board member of this journal, but he is not involved in the peer-review or decision of this article.

Author contribution statement

M. X. L.: Data curation, experimental design, material synthesis, validation, writing manuscript. C. L.: Data curation. H. Z.: Data curation. X. A. S.: Project administration. Z. R. S.: Project administration. D. C. P.: Project administration, funding acquisition, experimental design, writing manuscript. All the authors have approved the final manuscript.

Use of AI statement

None.

References

[1] Li, B.; Chen, F.; Xu, H. Y.; Song, Y.; Yan, X. H.; Xu, Q. L.; Wu, L. J.; Yan, Y. R.; Hou, W. J.; Cao, W. R. et al. *Nat. Rev. Electr. Eng.* **2024**, *1*, 412–425.

[2] Deng, Y. Z.; Peng, F.; Lu, Y.; Zhu, X. T.; Jin, W. X.; Qiu, J.; Dong, J. W.; Hao, Y. L.; Di, D. W.; Gao, Y. et al. Solution-processed green and blue quantum-dot light-emitting diodes with eliminated charge leakage. *Nat. Photonics* **2022**, *16*, 505–511.
[3] Fan, J. P.; Han, C. F.; Yang, G. J.; Song, B.; Xu, R.; Xiang, C. Y.; Zhang, T.; Qian, L. Recent progress of quantum dots light-emitting diodes: Materials, device structures, and display applications. *Adv. Mater.* **2024**, *36*, 2312948.
[4] Won, Y. H.; Cho, O.; Kim, T.; Chung, D. Y.; Kim, T.; Chung, H.; Jang, H.; Lee, J.; Kim, D.; Jang, E. Highly efficient and stable InP/ZnSe/ZnS quantum dot light-emitting diodes. *Nature* **2019**, *575*, 634–638.
[5] Shen, H. B.; Gao, Q.; Zhang, Y. B.; Lin, Y.; Lin, Q. L.; Li, Z. H.; Chen, L.; Zeng, Z. P.; Li, X. G.; Jia, Y. et al. Visible quantum dot light-emitting diodes with simultaneous high brightness and efficiency. *Nat. Photonics* **2019**, *13*, 192–197.
[6] Li, H.; Zhang, J. Y.; Wen, W.; Zhao, Y. Y.; Gao, H. F.; Ji, B. Q.; Wang, Y. J.; Jiang, L.; Wu, Y. C. Highly efficient light-emitting diodes via self-assembled InP quantum dots. *Nat. Commun.* **2025**, *16*, 4257.
[7] Jang, E.; Jang, H. Review: Quantum dot light-emitting diodes. *Chem. Rev.* **2023**, *123*, 4663–4692.
[8] He, S. Y.; Tang, X. Q.; Deng, Y. Z.; Yin, N.; Jin, W. X.; Lu, X. Y.; Chen, D. S.; Wang, C. Y.; Sun, T. L.; Chen, Q. et al. Anomalous efficiency elevation of quantum-dot light-emitting diodes induced by operational degradation. *Nat. Commun.* **2023**, *14*, 7785.
[9] Xiao, Z.; Zhang, M.; Ding, Y. H.; Shi, Z. Y.; Yin, Z. H.; Deng, H. H.; Meng, L. L.; Xu, B. J.; Liu, H. Solution-processed quantum dot micropatterns: From liquid manipulation to high-performance quantum dot light-emitting diode devices. *ACS Nano* **2025**, *19*, 10609–10619.
[10] Gao, Y.; Li, B.; Liu, X. N.; Shen, H. B.; Song, Y.; Song, J. J.; Yan, Z. J.; Yan, X. H.; Chong, Y. H.; Yao, R. Y. et al. Minimizing heat generation in quantum dot light-emitting diodes by increasing quasi-fermi-level splitting. *Nat. Nanotechnol.* **2023**, *18*, 1168–1174.
[11] Dai, X. L.; Zhang, Z. X.; Jin, Y. Z.; Niu, Y.; Cao, H. J.; Liang, X. Y.; Chen, L. W.; Wang, J. P.; Peng, X. G. Solution-processed, high-performance light-emitting diodes based on quantum dots. *Nature* **2014**, *515*, 96–99.
[12] Zhang, W. J.; Li, B.; Chang, C.; Chen, F.; Zhang, Q.; Lin, Q. L.; Wang, L.; Yan, J. H.; Wang, F. F.; Chong, Y. H. et al. Stable and efficient pure blue quantum-dot LEDs enabled by inserting an anti-oxidation layer. *Nat. Commun.* **2024**, *15*, 783.
[13] Li, M. Q.; Li, R.; Wu, L. J.; Lin, X. F.; Xia, X. Q.; Ao, Z. T.; Sun, X. J.; Chen, X. T.; Chen, S. Ultrabright and stable top-emitting quantum-dot light-emitting diodes with negligible angular color shift. *Nat. Commun.* **2024**, *15*, 5161.
[14] Song, J. J.; Wang, O. Y.; Shen, H. B.; Lin, Q. L.; Li, Z. H.; Wang, L.; Zhang, X. T.; Li, L. S. Over 30% external quantum efficiency light-emitting diodes by engineering quantum dot-assisted energy level match for hole transport layer. *Adv. Funct. Mater.* **2019**, *29*, 1808377.
[15] Xu, H. Y.; Song, J. J.; Zhou, P. H.; Song, Y.; Xu, J.; Shen, H. B.; Fang, S. C.; Gao, Y.; Zuo, Z. J.; Pina, J. M. et al. Dipole-dipole-interaction-assisted self-assembly of quantum dots for highly efficient light-emitting diodes. *Nat. Photonics* **2024**, *18*, 186–191.
[16] Lee, T.; Kim, B. J.; Lee, H.; Hahm, D.; Bae, W. K.; Lim, J.; Kwak, J. Bright and stable quantum dot light-emitting diodes. *Adv. Mater.* **2022**, *34*, 2106276.
[17] Zhu, X. T.; Luo, X.; Deng, Y. Z.; Wei, H.; Peng, F.; Ying, L.; Huang, F.; Hu, Y. Y.; Jin, Y. Z. Doping bilayer hole-transport polymer strategy stabilizing solution-processed green quantum-dot light-emitting diodes. *Sci. Adv.* **2024**, *10*, eado0614.
[18] Pu, C. D.; Dai, X. L.; Shu, Y. F.; Zhu, M. Y.; Deng, Y. Z.; Jin, Y. Z.; Peng, X. G. Electrochemically-stable ligands bridge the photoluminescence-electroluminescence gap of quantum dots. *Nat. Commun.* **2020**, *11*, 937.
[19] Shi, H. F.; Ren, Z. W.; Zheng, Z. Y.; Zhou, X.; Luo, C. Z.; Ji, H. F.; Zhang, Y. Z.; Chen, H.; Wu, C. L.; Chen, Y. Mercaptopropionic acid capped ZnMgO for efficient and stable quantum dot light-emitting diodes. *Laser Photonics Rev.* **2024**, *18*, 2400473.
[20] Chen, D. S.; Chen, D.; Dai, X. L.; Zhang, Z. X.; Lin, J.; Deng, Y. Z.; Hao, Y. L.; Zhang, C.; Zhu, H. M.; Gao, F. et al. Shelf-stable quantum-dot light-emitting diodes with high operational performance. *Adv. Mater.* **2020**, *32*, 2006178.
[21] Zheng, Y. Z.; Lin, X.; Li, J. Z.; Chen, J. N.; Wu, W. H.; Song, Z. X.; Gao, Y.; Hu, Z.; Wang, H. F.; Ye, Z. K. et al. *In situ* n-doped nanocrystalline electron-injection-layer for general-lighting quantum-dot LEDs. *Nat. Commun.* **2025**, *16*, 3362.
[22] Chen, D. S.; Ma, L. Y.; Chen, Y. H.; Zhou, X. Q.; Xing, S. Y.; Deng, Y. Z.; Hao, Y. L.; Pu, C. D.; Kong, X. Q.; Jin, Y. Z. Electrochemically stable ligands of ZnO electron-transporting layers for quantum-dot light-emitting diodes. *Nano Lett.* **2023**, *23*, 1061–1067.
[23] Luo, C. Z.; Zheng, Z. S.; Ding, Y. H.; Ren, Z. W.; Shi, H. F.; Ji, H. F.; Zhou, X.; Chen, Y. High-resolution, highly transparent, and efficient quantum dot light-emitting diodes. *Adv. Mater.* **2023**, *35*, 2303329.
[24] Wang, S.; Liu, S. H.; Wang, T.; Bai, J. L.; Peng, J. Y.; Zhang, H. Z.; Xie, W. F.; Ji, W. Y. Operando ZnO recrystallization for efficient quantum-dot light-emitting diodes. *Light Sci. Appl.* **2025**, *14*, 196.
[25] Chen, Z. N.; Su, Q.; Qin, Z. Y.; Chen, S. M. Effect and mechanism of encapsulation on aging characteristics of quantum-dot light-emitting diodes. *Nano Res.* **2021**, *14*, 320–327.
[26] Acharya, K. P.; Titov, A.; Hyvonen, J.; Wang, C. G.; Tokarz, J.; Holloway, P. H. High efficiency quantum dot light emitting diodes from positive aging. *Nanoscale* **2017**, *9*, 14451–14457.
[27] Chen, Z. N.; Chen, S. M. Eliminating positive aging in quantum dot light-emitting diodes by H_2O-treatment. *Adv. Mater.* **2025**, *37*, 2503477.
[28] Ke, W. J.; Fang, G. J.; Liu, Q.; Xiong, L. B.; Qin, P. L.; Tao, H.; Wang, J.; Lei, H. W.; Li, B. R.; Wan, J. W. et al. Low-temperature solution-processed tin oxide as an alternative electron transporting layer for efficient perovskite solar cells. *J. Am. Chem. Soc.* **2015**, *137*, 6730–6733.
[29] Yang, C. Y.; Ma, R.; Wang, Z.; Wang, Y. Y.; Yu, C. Y.; Liu, Y. G.; Wan, Y. F.; Li, J. F.; Tong, J. F.; Zhang, P. et al. Efficient quantum dot light-emitting diode enabled by a thick inorganic CdS interfacial modification layer. *ACS Appl. Mater. Interfaces* **2023**, *15*, 54185–54191.
[30] Chen, Z. N.; Chen, S. M. Efficient and stable quantum-dot light-emitting diodes enabled by tin oxide multifunctional electron transport layer. *Adv. Opt. Mater.* **2022**, *10*, 2102404.
[31] Yang, G.; Lei, H. W.; Tao, H.; Zheng, X. L.; Ma, J. J.; Liu, Q.; Ke, W. J.; Chen, Z. L.; Xiong, L. B.; Qin, P. L. et al. Reducing hysteresis and enhancing performance of perovskite solar cells using low-temperature processed Y-doped SnO_2 nanosheets as electron selective layers. *Small* **2017**, *13*, 1601769.
[32] Liu, Y.; Wei, S.; Wang, G.; Tong, J. Y.; Li, J.; Pan, D. C. Quantum-sized SnO_2 nanoparticles with upshifted conduction band: A promising electron transportation material for quantum dot light-emitting diodes. *Langmuir* **2020**, *36*, 6605–6609.
[33] Feng, H. W.; Liu, S. H.; Tang, G.; Zhang, L. T.; Xie, W. F. Highly efficient and stable quantum dot light-emitting devices with a low-temperature tin oxide electron transport layer. *J. Mater. Chem. C* **2021**, *9*, 13748–13754.
[34] Chen, M. Y.; Chen, X. T.; Ma, W. C.; Sun, X. J.; Wu, L. J.; Lin, X. F.; Yang, Y. X.; Li, R.; Shen, D. Y.; Chen, Y. et al. Highly stable SnO_2-based quantum-dot light-emitting diodes with the conventional device structure. *ACS Nano* **2022**, *16*, 9631–9639.
[35] Gao, J. X.; Liu, M. X.; Shi, X. N.; Pan, D. C. Ligand-assisted solvothermal precipitation synthesis of quantum-sized SnO_2

nanoparticles and their application in quantum dot light emitting diodes. *New J. Chem.* **2024**, *48*, 8631–8637.
[36] Ma, W. C.; Ren, Z. W.; Shi, H. F.; Xia, X. Q.; Wang, X. W.; Ji, H. F.; Chen, H.; Luo, C. Z.; Wang, C. H.; Chen, S. et al. Manganese doped tin oxide for stable and efficient quantum dot light-emitting diodes. *Laser Photonics Rev.* **2024**, *18*, 2400005.
[37] Zhao, J. X.; Man, Z. W.; Wang, S. B.; Hao, C. Q.; Yu, Z. Z.; Li, X.; Tang, A. W. Enhanced performance of quantum dot light-emitting diodes enabled by zirconium-doped SnO_2 as electron transport layers. *Opt. Lett.* **2024**, *49*, 1896–1899.
[38] Huang, Y. J.; Cao, S.; Liang, Y.; Li, Q. Y.; Chen, Z. T.; Lai, C. L.; Zou, B. S.; Zhao, J. L. High-efficiency and stable ZnSeTe-based blue QLEDs enabled by freeze-dried SnO_2 nanoparticle interlayers. *Laser Photonics Rev.* **2025**, *19*, 2500049.
[39] Wang, Y. C.; Zhang, H. Z.; Ji, W. Y. Efficient quantum-dot light-emitting diodes based on solvent-annealed SnO_2 electron-transport layers. *ACS Appl. Electron. Mater.* **2023**, *5*, 537–543.
[40] Xia, X. Q.; Chen, X. T.; Xie, J. C.; Li, X. R.; Chen, S. Decoupling the conductivity-fluorescence tradeoff of SnO_2 nanocrystals for efficient and stable quantum dot light-emitting diodes. *Laser Photonics Rev.* **2025**, *19*, 2401755.
[41] Luo, L.; Fan, Z.; Zhang, Z. B.; Liu, D. Y.; Li, G. F.; Wang, L. S.; Zou, B. S. Zn-doped SnO_2 NPs as electron transport layer in green CdSe/ZnS quantum dot light-emitting diodes. *ACS Appl. Nano Mater.* **2024**, *7*, 7934–7943.
[42] Liu, M. X.; Lin, C.; Li, H. W.; Pan, J. J.; Liu, Y. H.; Su, X.; Shi, X. N.; Zhang, H.; Zou, B. S.; Pan, D. C. Positive aging-free SnO_2-based quantum dot light-emitting diodes with average external quantum efficiency exceeding 24%. *Adv. Funct. Mater.* **2026**, *36*, e15270.
[43] Lin, C.; Liu, M. X.; Liu, Y. H.; Shi, X. N.; Pan, D. C. Tuning charge transportation balance in quantum dot light emitting diodes by decreasing the mobility and conductivity of In-doped SnO_2 nanocrystal electron transport layers. *Dalton Trans.* **2025**, *54*, 5511–5520.
[44] Lei, S. Y.; Xiao, Y. Y.; Yu, K. L.; Xiao, B.; Wan, M.; Zou, L. Y.; You, Q. L.; Yang, R. Q. Revisiting hole injection in quantum dot light-emitting diodes. *Adv. Funct. Mater.* **2023**, *33*, 2305732.
[45] Schwenn, P. E.; Gui, K.; Nardes, A. M.; Krueger, K. B.; Lee, K. H.; Mutkins, K.; Rubinstein-Dunlop, H.; Shaw, P. E.; Kopidakis, N.; Burn, P. L. et al. A small molecule non-fullerene electron acceptor for organic solar cells. *Adv. Energy Mater.* **2011**, *1*, 73–81.
[46] Ko, Y.; Kim, Y.; Lee, C.; Kim, Y.; Jun, Y. Investigation of hole-transporting poly(triarylamine) on aggregation and charge transport for hysteresisless scalable planar perovskite solar cells. *ACS Appl. Mater. Interfaces* **2018**, *10*, 11633–11641.
[47] Cao, W. R.; Xiang, C. Y.; Yang, Y. X.; Chen, Q.; Chen, L. W.; Yan, X. L.; Qian, L. Highly stable QLEDs with improved hole injection via quantum dot structure tailoring. *Nat. Commun.* **2018**, *9*, 2608.
[48] Cai, F. S.; Zong, H.; Li, M.; Li, C. G.; Huang, G. G.; Pascual, J.; Liang, C.; Su, Z. H.; Li, Z.; Gao, X. Y. et al. Charge carrier regulation for efficient blue quantum-dot light-emitting diodes via a high-mobility coplanar cyclopentane[*b*]thiopyran derivative. *Nano Lett.* **2024**, *24*, 5284–5291.
[49] Li, B.; Fang, Y. F.; Bai, P. L.; Wang, Y. Q.; Li, J. Y.; Xiao, B. B.; Wang, Y. P. Effect of PVK mixed TAPC as hole transport layers on device performance of red quantum-dot light-emitting diodes. *J. Lumin.* **2022**, *247*, 118871.
[50] Liu, Y. Y.; Lan, L. H.; Liu, B. C.; Tao, H.; Li, M.; Xu, H.; Zou, J. H.; Xu, M.; Wang, L.; Peng, J. B. et al. Improved performance of inverted quantum dot light-emitting diodes by blending the small-molecule and polymer materials as hole transport layer. *Org. Electron.* **2020**, *80*, 105618.
[51] Abbaszadeh, D.; Kunz, A.; Kotadiya, N. B.; Mondal, A.; Andrienko, D.; Michels, J. J.; Wetzelaer, G. J. A. H.; Blom, P. W. M. Electron trapping in conjugated polymers. *Chem. Mater.* **2019**, *31*, 6380–6386.
[52] Ehrenfreund, E.; Lungenschmied, C.; Dennler, G.; Neugebauer, H.; Sariciftci, N. S. Negative capacitance in organic semiconductor devices: Bipolar injection and charge recombination mechanism. *Appl. Phys. Lett.* **2007**, *91*, 012112.
[53] Li, Q. Y.; Cao, S.; Bi, Y. H.; Song, Y. S.; Liang, Y.; Li, H. Y.; Xing, K.; Zou, B. S.; Zhao, J. L. Dipole modulation engineering enhances structural order of PEDOT: PSS for efficient and stable InP-based QLEDs. *ACS Appl. Mater. Interfaces* **2024**, *16*, 70728–70736.
[54] Qu, X. W.; Ma, J. R.; Wang, K.; Sun, X. W. Characteristic voltages and times from capacitance-voltage analysis of quantum dot light-emitting diodes. *Appl. Phys. Lett.* **2024**, *124*, 263503.